Twenty-Seventh Symposium (International) on Combustion/The Combustion Institute, 1998/pp. 971–978

THE DOMAIN OF INFLUENCE OF FLAME INSTABILITIES IN TURBULENT PREMIXED COMBUSTION

H. BOUGHANEM AND A. TROUVÉ
Centre de Recherche en Combustion Turbulente
Institut Français du Pétrole
92852 Rueil-Malmaison, France

Although a number of experiments and numerical simulations indicate persistence of flame instability effects in turbulent premixed flames, the exact domain of influence of these instabilities remains unknown. In this study, a simple estimate of that domain is obtained by comparing a characteristic flame stretch due to flame instabilities, K_i, with a characteristic flame stretch due to turbulent eddies, K_t. The resulting criterion, $(K_t/K_i) \leq 1$, shows that instability effects are promoted by: small values of the ratio of turbulence intensity divided by the laminar flame speed (u'/s_L); large values of the ratio of integral length scale divided by the laminar flame thickness (l_t/l_F) (given that $(l_t/l_F) > 10$); large values of the heat release factor τ; large positive values of the flame Richardson number *Ri* (*Ri* measures buoyancy effects and is positive when the corresponding flow acceleration is directed from the fresh mixture to the burnt gas); small values (below one) of the flame Lewis number *Le*.

Direct numerical simulations (DNS) are used to test the validity of the theoretical criterion. The numerical configuration corresponds to three-dimensional premixed flames propagating into a temporally decaying turbulent flow. The simulations are limited by DNS constraints to small length scale ratios, $(l_t/l_F) \leq 10$; they use $Le = 1$ and correspond to different values of (u'/s_L), τ and *Ri*. Due to the turbulence decay, all simulated flames with $\tau \neq 0$ and $Ri \geq 0$ undergo a transition from turbulent to unstable flame surface dynamics. The DNS values of (K_t/K_i) at transition time are found to be of order one and are in good agreement with the theoretical predictions.

Introduction

The classical stability theory of laminar flames reveals that the propagation of a premixed flame front has a marked tendency to become unstable [1–5]. The instability mechanisms are of several types: gas expansion effects are responsible for the hydrodynamic Darrieus–Landau instability; buoyancy effects are responsible for the Taylor instability; molecular diffusion effects are responsible for the diffusive-thermal instability. Laminar premixed flame instabilities are promoted by: (1) large values of the heat release factor, $\tau \equiv (T_b - T_u)/T_u$, where T_u (T_b) is the unburnt (burnt) gas temperature; (2) positive values of the flame Richardson number, $Ri \equiv (\Gamma D_{th}/\tau s_L^3)$, where Γ is the amplitude of an externally imposed acceleration field (for instance, gravity), with $\Gamma > 0$ when directed from the fresh mixture to the burnt gas, and where D_{th} is the thermal diffusivity and s_L the laminar flame speed; (3) small values (below one) of the flame Lewis number, $Le \equiv (D_{th}/D)$, where D is the mass diffusivity of the deficient reactant. Unstable flames propagating in uniform laminar flows feature unsteady flame front motions, flame surface wrinkling and overall flame speeds larger than s_L.

For premixed flames propagating in turbulent flows, flame instability effects combine with effects due to the turbulent motions. The coupling between the flame and turbulence dynamics has been described using asymptotic theory in a series of related studies [6–8]. These studies indicate that turbulent flame propagation depends on both the incoming flow properties and the stability properties of the wrinkled laminar flame surface. For instance, the turbulent flame speed is found to be a function of both turbulent scales and flame parameters like τ, *Ri*, and *Le*. These analytical studies, however, are restricted to intrinsically stable flames that are linearly perturbed by weakly turbulent flows. The restriction to stable systems and linear dynamics explains why basic results from laminar flame stability theory are not easily incorporated into statistical models of turbulent combustion. In turbulent combustion models, whereas the effects of diffusive-thermal phenomena are sometimes included (see, for instance, Ref. [9]), the effects of the Darrieus–Landau instability are usually neglected.

This situation is far from satisfactory as experiments [10,11] and numerical simulations [12–15] indicate persistence of flame instability effects in turbulent flames, at low or high Reynolds numbers, and thereby shed a critical light on the traditional assumption that turbulent fluctuations have sufficient

energy to overpower flame instabilities. A critical evaluation of this assumption can be found in recent studies by Cambray and Joulin [16] and Paul and Bray [17]. The numerical and analytical study by Cambray and Joulin removes the restriction of previous theoretical work to stable flames and linear dynamics and thereby provides new valuable information for statistical models. It provides in particular a unique description of the characteristic length scale of flame surface wrinkling in the fully developed nonlinear regime reached by unstable (weakly) turbulent flames. This description is used in Ref. [17] to incorporate full flame instability effects in a modified flame surface density model. Preliminary results from the model suggest that flame instability effects are important under low-intensity turbulent conditions, $(u'/s_L) < 1$, where u' is the turbulent rms velocity. Although $(u'/s_L) < 1$ is a valuable first-order estimate of the domain of influence of flame instabilities in turbulent premixed combustion, it clearly does not account for the effects of turbulent length scales or flame parameters like τ, Ri, and Le. The exact domain of influence of flame instabilities remains unknown.

The objective of this paper is to provide an estimate of that domain. This estimate is based on the modeling strategy proposed by Paul and Bray [17] as well as closure models to measure flame stretch due to flame instabilities, K_i, and flame stretch due to turbulent eddies, K_t. The domain of influence of flame instabilities corresponds to the simple criterion $(K_t/K_i) \leq 1$ and is presented in the next section. Direct numerical simulation (DNS) of premixed flames in isotropic turbulent flow are then used in the remainder of the paper to test the new criterion. The DNS database corresponds to various values of (u'/s_L), τ, and Ri.

Theory

The present theory is based on the classical flamelet description of turbulent flames as thin surfaces separating fresh reactants and burnt products, and a model description of the different contributions to flame surface wrinkling. A convenient framework to study flame wrinkling is the exact evolution equation for the flame surface density Σ [18,19]. In the present work, we choose to consider the coherent flame model (CFM) based on a modeled formulation of the Σ-equation [20–22]:

$$\frac{\partial \Sigma}{\partial t} + \frac{\partial}{\partial x_i}(\tilde{u}_i \Sigma) = \frac{\partial}{\partial x_i}\left(D_t \frac{\partial \Sigma}{\partial x_i}\right) + \alpha K \Sigma - \beta \frac{s_L \Sigma^2}{\bar{c}(1-\bar{c})} \quad (1)$$

where $\tilde{u}_i$ is the Favre-averaged flow velocity, D_t a turbulent diffusivity, K the total flame stretch, $\bar{c}$ the Reynolds-averaged reaction progress variable, and α and β are model constants. The three terms on the right-hand side of equation 1 correspond respectively to transport of Σ by the turbulent fluctuations, production of Σ by flame stretch, and dissipation of Σ by flame propagation effects. The production term can be decomposed into two components [17]: a first component that accounts for flame instability effects and a second component that accounts for straining due to the turbulent motions, $\alpha K \Sigma = \alpha K_i \Sigma + \alpha K_t \Sigma$. The turbulent component of flame stretch K_t has received a lot of attention in the literature because this component is responsible for flame surface augmentation by turbulence. In CFM, K_t is written as:

$$K_t = \left(\frac{\varepsilon}{\nu}\right)^{1/2} \gamma_k \quad (2)$$

where ε is the mean (Favre-averaged) rate of dissipation of turbulent kinetic energy, $\varepsilon \equiv 0.42\,(k^{3/2}/l_t)$, with k the mean turbulent kinetic energy, $k \equiv 1.5u'^2$, and l_t the integral length scale of the turbulent flow, and where ν is the kinematic viscosity and γ_k a model function proposed by Meneveau and Poinsot [24]. In Ref. 24, γ_k is described as a function of the relative flow to flame velocity and length scale ratios, (u'/s_L) and (l_t/l_F), where $l_F \equiv (D_{th}/s_L)$ is the laminar flame thickness.

The flame instability component of flame stretch K_i is more difficult to model. Following Paul and Bray [17], we first consider the approximation *production = dissipation* in equation 1 and find an algebraic closure expression for Σ:

$$\Sigma = \frac{\alpha}{\beta} \frac{K\,\bar{c}(1-\bar{c})}{s_L} \quad (3)$$

We also use the Bray–Moss–Libby (BML) relation [23] between the flame surface density and the characteristic length scale of wrinkling $\hat{L}_y$:

$$\Sigma = \frac{g}{\bar{\sigma}_y} \frac{\bar{c}(1-\bar{c})}{\hat{L}_y} \quad (4)$$

where g is a model constant and $\bar{\sigma}_y$ is the flamelet orientation factor, also assumed to be a constant. When equations 3 and 4 are combined, a simple relation between flame stretch and length scale of wrinkling is obtained:

$$K = a \frac{s_L}{\hat{L}_y} \quad (5)$$

where $a \equiv (g\beta/\sigma_y\alpha)$. Equation 5 is used in Ref. [17] to translate the results of Cambray and Joulin [16] into a model for flame stretch due to flame instabilities. A similar strategy is adopted here. In the limiting case of low-intensity turbulence, $(u'/s_L) \to 0$, equation 5 becomes

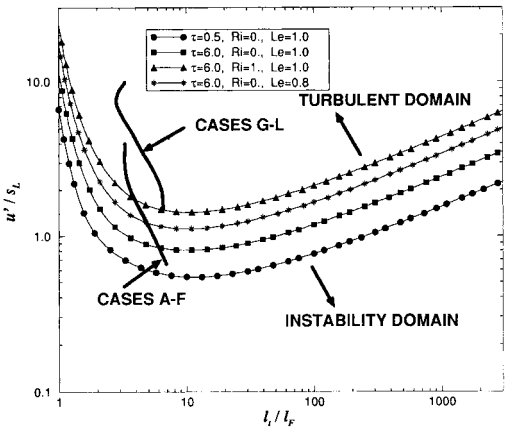

FIG. 1. Limit of the domain of influence of flame instabilities in a turbulent combustion diagram parametrized by $(l_t/l_F, u'/s_L)$ (Eq. 8). The limit is plotted for different values of τ, Ri and Le. Also plotted are the time evolving conditions of the present direct numerical simulations (Table 1).

$$K_i = a \frac{s_L}{\hat{L}_y} \tag{6}$$

where $\hat{L}_y$ is the length scale of wrinkling studied in Ref. [16]. Now, although an elaborate model for $\hat{L}_y$ is proposed by Cambray and Joulin, an important result is that this length scales like the marginally stable wavelength Λ_n of the linearized unforced flame stability theory. It then follows that a simple estimate of K_i is

$$K_i = a \frac{s_L}{\Lambda_n} \tag{7}$$

where Λ_n is a known function of flame parameters like τ, Ri, and Le, as given in Ref. [3].

Finally, combining equations 2 and 7, the domain of influence of flame instabilities can be estimated by the following condition:

$$\frac{K_t}{K_i} = A \left(\frac{u'}{s_L}\right)^{3/2} \left(\frac{l_t}{l_F}\right)^{-1/2} \left(\frac{\Lambda_n}{l_F}\right) \gamma_k \leq 1 \tag{8}$$

where $A \equiv (0.42^{1/2} 1.5^{3/4})/(aPr^{1/2})$ and Pr is the Prandtl number. The criterion $(K_t/K_i) = 1$ is plotted in Fig. 1 in a classical diagram for turbulent premixed combustion. The model constants are $\alpha = 2.1, \beta = 1, g = 1.5, \bar{\sigma}_y = 0.7, Pr = 0.75$. Consistent with previous results [16,17], instability effects are promoted by small values of (u'/s_L). The limit between unstable and turbulent flames also depends on (l_t/l_F). As $(l_t/l_F) \to \infty$, $\gamma_k \to 0.28$ [24], and the limit becomes a straight line in the log-log plot with a slope 1/3. As $(l_t/l_F) \to 0$, γ_k takes decreasing values [24] and the instability domain becomes significantly larger. In Fig. 1, the criterion is also plotted for different values of τ, Ri, and Le. Consistent with results from flame stability theory [1–5], instability effects are promoted by large values of τ, large positive values of Ri, and small values of Le.

DNS of Stable/Unstable Turbulent Flames

Numerical Methods and Configuration

The simulations use a three-dimensional, compressible Navier–Stokes solver. The solver features a high-order finite difference scheme that is sixth-order accurate in space [25] and third-order accurate in time; boundary conditions are specified with a method proposed by Poinsot and Lele [26]. The chemistry model is a single-step, irreversible chemical reaction where the reaction rate depends exponentially on temperature (Arrhenius kinetics). The nondimensional reaction rate is written as [15]:

$$\dot{\omega}_R = B\rho Y_R \exp\left(\frac{-Ze(1-\Theta)}{1-\gamma(1-\Theta)}\right) \tag{9}$$

where ρ is the mass density, Y_R the reactant mass fraction, and Θ the reduced temperature, $\Theta \equiv (T - T_u)/(T_b - T_u)$. The coefficients B, γ, and Ze are, respectively, the reduced preexponential factor; the modified heat release factor, $\gamma \equiv \tau/(\tau + 1)$; and the reduced activation energy, $Ze \equiv \gamma(T_a/T_b)$, with T_a the activation temperature. In the present simulations, $Ze = 8.0$, whereas B and γ take different values (Table 1). The values of B are chosen so that s_L remains constant throughout all simulated cases. Also, $Pr = 0.75$ and $Le = 1$.

The computational configuration corresponds to a premixed flame embedded in a three-dimensional, decaying, isotropic turbulent flow. It is identical to the configuration studied by Veynante and Poinsot [27] (see also Ref. [15]). The calculations are initialized with fresh reactants on the left-hand side of the domain ($x_1 < 0$) and burnt products on the right ($x_1 > 0$); the two are separated by a plane laminar flame. Isotropic turbulence is initially specified according to a model energy spectrum. The left- and right-hand sides of the computational domain are inflow and outflow boundaries, whereas periodic boundary conditions are applied at lateral walls. Note that no turbulence is generated at the inflow boundary, and the simulations are time evolving rather than space evolving. For cases with $Ri \neq 0$, a body force term corresponding to a constant acceleration is included in the momentum and energy equations [27].

Values of the run parameters are reported in Table 1. At time $t = 0$, the turbulence is characterized by moderate (cases A–F) or high (cases G–L) turbulence intensities and length scales that are slightly larger than the flame thickness. Because the present simulations feature decaying turbulence, the DNS characteristics are time evolving: they are represented by line segments in Fig. 1. Typically, at time

TABLE 1
Dimensionless parameters for the simulations

Case	B	τ	Ri	u'/S_L	l_t/l_F	Re_t	l_t/Λ_n	t_1/τ_0	$K_t/K_i(t = t_1)$
A	38.0	0.5	0.0	4.0	3.3	18.0	0.07	4.1	2.0
B	93.2	2.0	0.0	4.0	3.3	18.0	0.12	2.8	1.6
C	166.0	4.0	0.0	4.0	3.3	18.0	0.13	2.1	1.8
D	238.7	6.0	0.0	4.0	3.3	18.0	0.13	1.8	2.0
E	238.7	6.0	1.0	4.0	3.3	18.0	0.27	1.4	1.1
F	238.7	6.0	−1.0	4.0	3.3	18.0	*na*	*na*	—
G	38.0	0.5	0.0	10.0	3.3	45.0	0.07	*no*	—
H	93.2	2.0	0.0	10.0	3.3	45.0	0.12	*no*	—
I	166.0	4.0	0.0	10.0	3.3	45.0	0.13	6.7	3.3
J	238.7	6.0	0.0	10.0	3.3	45.0	0.13	5.6	3.6
K	93.2	2.0	6.0	10.0	3.3	45.0	0.45	6.6	1.0
L	93.2	2.0	−6.0	10.0	3.3	45.0	*na*	*na*	—

The reduced preexponential factor B is made nondimensional by the laminar flame time (D_{th}/s_L^2). Reported values of (u'/s_L), (l_t/l_F), $Re_t \equiv (u'l_t/\nu)$ and (l_t/Λ_n) correspond to initial conditions. In the first and second from last columns, *na* stands for *not applicable* and *no* for *not observed.*

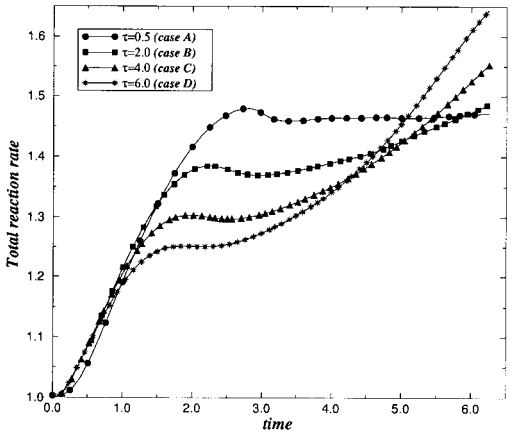

FIG. 2. Effects of gas expansion on the overall reaction rate (cases A–D). The overall reaction rate $\langle\dot{\omega}_R\rangle$ is made non-dimensional by its initial value corresponding to a strain-free, plane laminar flame. Time is made non-dimensional by the initial turbulent eddy turnover time τ_0.

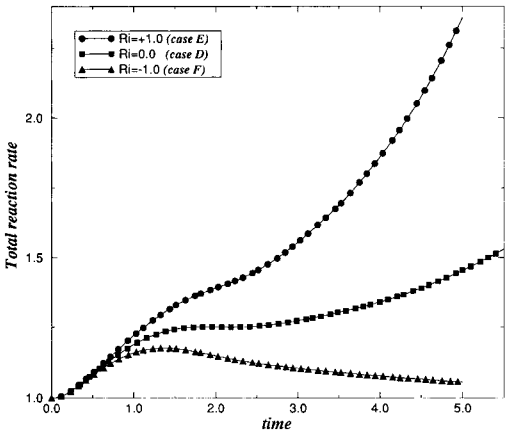

FIG. 3. Buoyancy effects on the overall reaction rate (cases D–F). The overall reaction rate $\langle\dot{\omega}_R\rangle$ is made non-dimensional by its initial value corresponding to a strain-free, plane laminar flame. Time is made non-dimensional by the initial turbulent eddy turnover time τ_0.

$t/\tau_0 = 4$, where τ_0 is the initial turbulent eddy turnover time, (u'/s_L) has decreased by a factor of 3, whereas (l_t/l_F) has slightly increased. Note that l_t is initially nine times smaller than the size of the (cubic) computational domain. Note also that the assumption of large length scales used in flame stability theory is not satisfied in the DNS ($l_t/\Lambda_n < 1$). The limitation to small eddy sizes is due to the severe resolution requirements associated with DNS [28]. In the present work, the grid spacing is uniform and the resolution is 150^3.

Results

The simulations describe the wrinkling of the flame surface by turbulent motions as well as by possible instability effects. Figs. 2 and 3 present typical time evolutions of the overall reaction rate, $\langle\dot{\omega}_R\rangle(t) \equiv (\int \dot{\omega}_R(x_i, t)dV)/V$, where V is the volume of the computational domain. Such variations are related to modifications of the total flame surface area [13–15]. One may distinguish three phases in Figs. 2 and 3: (1) a transient phase ($t/\tau_0 \leq 2$) where the turbulence wrinkles the initially flat flame surface; (2) a

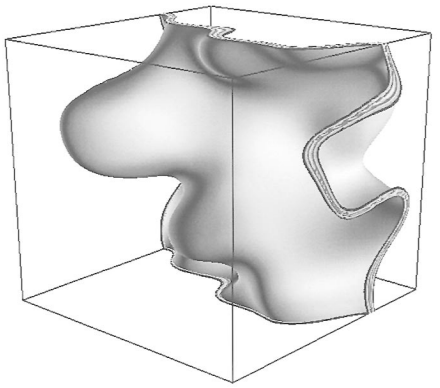

FIG. 4. Snapshot of the flame surface contour ($c = 0.8$) at time $t/\tau_0 = 4.75$. Case E ($\tau = 6.0$, $Ri = 1.0$). The flow is from bottom-left (reactants) to top-right (products).

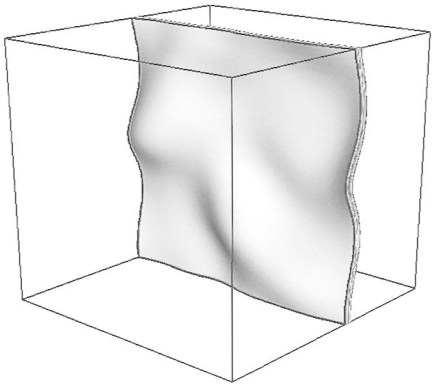

FIG. 5. Snapshot of the flame surface contour ($c = 0.8$) at time $t/\tau_0 = 4.75$. Case F ($\tau = 6.0$, $Ri = -1.0$). The flow is from bottom-left (reactants) to top-right (products).

turbulent phase where the flame and flow are in equilibrium and the flame surface becomes smoother in response to the turbulence decay; and (3) a stable/unstable phase where, depending on the values of τ and Ri, the flame surface area either relaxes to its initial state (case F) or keeps increasing in time without saturation (cases B–E). In cases B–E, whereas saturation of $\langle\dot{\omega}_R\rangle(t)$ might be expected at later times, the simulations are limited by the size of the computational domain, and this subsequent phase is not observed. The simulations, however, indicate that saturation will not occur on a timescale characteristic of the turbulence. In that sense, the flames in cases B–E can be qualified as unstable. Also, although a transition to a stable/unstable phase is not observed in case A of Fig. 2, it was determined using a second longer DNS run that case A features a sudden increase in overall reaction rate after $t/\tau_0 \approx 6$. Thus, all simulated flames with $\tau \neq 0$ and $Ri \geq 0$ are found to undergo a transition to unstable behavior.

Figure 2 gives a good illustration of the rich variety of observable effects in the DNS. For instance, the effects of τ on the overall reaction rate are reversed in the turbulent and unstable phases of the simulations. In the unstable phase, consistent with results from flame stability theory [1–5], large values of τ promote the onset of the Darrieus–Landau instability and tend to increase $\langle\dot{\omega}_R\rangle$. On the contrary, in the turbulent phase of the simulations (at earlier times), large values of τ tend to decrease the flame surface wrinkling and turbulent flame speed. It is worth emphasizing that this apparent turbulent effect of τ on the overall reaction rate is at odds with the BML theory [29]. To date, it remains unexplained. Consistent with BML predictions, large values of τ are found to promote countergradient diffusion in the turbulent transport of mean reaction progress variable [29,30]. However, whereas countergradient diffusion effects might account for modifications in the turbulent flame structure, such modifications are not expected to lead to changes in the turbulent flame speed when $Ri = 0$ [29]. The discrepancy between the DNS results and BML predictions illustrated by Fig. 2 is an interesting finding of the present study. It is somewhat beyond the scope of this paper and will be addressed in future work.

In contrast to the conflicting effects of τ, the turbulent and unstable effects of Ri have a similar influence on the overall reaction rate (Fig. 3). This influence is consistent with predictions from both the BML [31] and the laminar flame stability [1–5] theories. Positive (negative) values of Ri promote gradient (countergradient) turbulent scalar transport [31,27] as well as unstable (stable) buoyancy effects [1–5] and lead to increased (decreased) flame surface wrinkling. In fact, the differences between Taylor stable and Taylor unstable systems are so pronounced that they can easily be observed in the simulations by comparing instantaneous snapshots of the flame surface (Figs. 4 and 5).

Further evidence of a transition in the simulations from turbulent to intrinsic flame dynamics is presented in Figs. 6 and 7. These figures show a comparison between a characteristic strain rate of the turbulent flow a_M and a characteristic flame stretch K_+. Following Yeung et al. [32], $a_M \equiv 0.28\ (\varepsilon/\nu)^{1/2}$, which corresponds to the mean strain rate acting on a material surface in isotropic turbulence. Also, $K_+ \equiv \int_0^\infty \kappa p(\kappa) d\kappa$, where $p(\kappa)$ is the probability density function of flame stretch κ. $p(\kappa)$ is readily obtained from the simulations [15] and K_+ gives a simple estimate of the mean rate of flame surface production. In a stationary flame, positive stretch values contributing to K_+ are exactly balanced by negative stretch values, and the net effect on the flame surface is zero. Furthermore, according to Ref. [24], *in situ*ations where the flame wrinkling is controlled by the

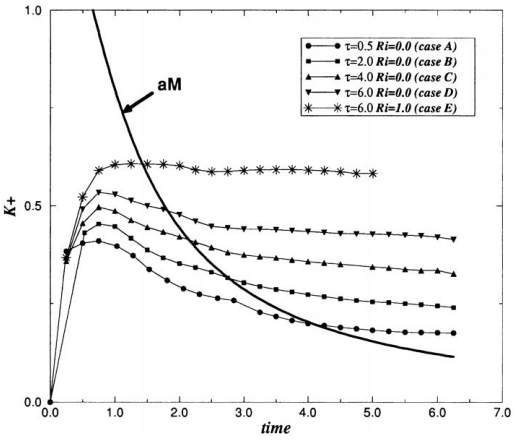

FIG. 6. Comparison between the characteristic strain rate of the turbulent flow a_M and the characteristic flame stretch K_+ (cases A–E). All quantities are made non-dimensional by the initial turbulent eddy turnover time τ_0.

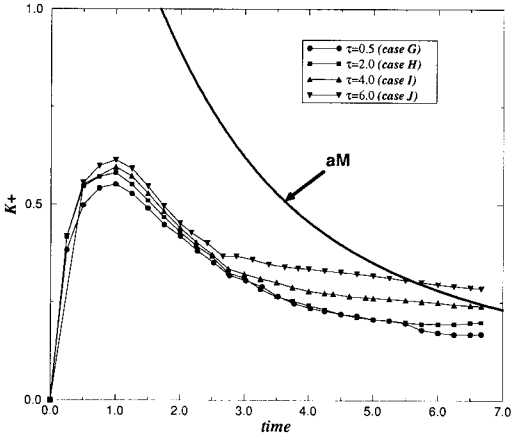

FIG. 7. Comparison between the characteristic strain rate of the turbulent flow a_M and the characteristic flame stretch K_+ (cases G–J). All quantities are made non-dimensional by the initial turbulent eddy turnover time τ_0.

turbulent eddies, the rate of production of flame surface area is always less than the rate of production of material surface area, $K_+ \leq a_M$. Figs. 6 and 7 show that due to the turbulence decay, this relation only holds for a limited time in the simulations. Flame-flow conditions where $K_+ \geq a_M$ indicate transition to an unstable regime where flame stretch becomes unrelated to the turbulent velocity field and where the flame wrinkling is controlled by intrinsic flame dynamics. The condition $(K_+/a_M) = 1$ is conveniently used to estimate when the transition occurs. Consistent with previous observations, large values of τ and positive values of Ri produce strong flame instabilities and promote an early transition (Fig. 6), whereas large values of (u'/s_L) produce strong turbulent effects and delay the transition (Fig. 7). Values of the transition time t_1 are reported in Table 1.

These results can also be used for a quantitative test of the theoretical criterion in equation 8. Each case in the DNS database is probed to determine if and when transition to unstable flame dynamics occurs in the course of the simulations ($t/\tau_0 < 7$). Note that the definition of t_1 is believed to be inadequate to the analysis of stable systems and is not used for cases F and L where $Ri < 0$. For the other cases, the value of (K_t/K_i) is computed at time $t = t_1$ and reported in the last column of Table 1. It is found that consistent with the theoretical predictions of equation 8, transition from turbulent to unstable flame behavior is observed in the DNS for values of the stretch ratio of order one, $1.0 \leq (K_t/K_i)\ (t = t_1) \leq 3.6$. These values, however, are higher than one, which suggests that the theoretical criterion underestimates the domain of influence of flame instabilities. Also, there is some scatter in the values taken by $(K_t/K_i)\ (t = t_1)$. Given the uncertainties associated with the definition of t_1, this scatter is difficult to interpret and is deemed acceptable.

Conclusion

A model description of the different contributions to flame surface wrinkling is used in this study to propose a simple criterion that estimates the domain of influence of flame instabilities in turbulent premixed combustion (equation 8). This criterion suggests that the occurrence of flame instabilities in turbulent configurations is determined by the relative flow to flame velocity and length scale ratios, (u'/s_L) and (l_t/l_F), and by flame parameters like τ, Ri, and Le. Note that based on this criterion, and consistent with some experimental results [10,11], flame instabilities are predicted at high turbulent Reynolds numbers.

Direct numerical simulations (DNS) of premixed flames in decaying turbulence are then used to test the theory. It is found that due to the turbulence decay, all simulated cases undergo a transition to stable or unstable flame behavior. In particular, all cases with $\tau \neq 0$ and $Ri \geq 0$ become unstable. The DNS database provides a good illustration of the many different dynamical effects associated with gas expansion or buoyancy. In the turbulent phase, large values of τ (large positive values of Ri) promote countergradient (gradient) diffusion of mean reaction progress variable and tend to decrease (increase) the flame surface wrinkling. Although the turbulent effect of Ri on the overall reaction rate is consistent with the BML theory, the apparent turbulent effect of τ remains inconsistent and unexplained. In the unstable phase of the simulations,

consistent with results from laminar flame stability theory, large values of τ (large positive values of Ri) promote the onset of the Darrieus–Landau (Taylor) instability and tend to increase the flame surface wrinkling. Finally, the analysis of when transition from turbulent to unstable flame dynamics occurs in the DNS produces results that are in good agreement with the proposed criterion in equation 8.

Note also that from a DNS perspective, because the effects of important parameters like τ are reversed in the turbulent and unstable phases of the simulations, it is believed that failure to identify transition from one regime to the other is a potential source of error and misinterpretation. In fact, the criterion proposed in this study suggests that flame instabilities occur over a significant portion of the domain of flame-flow conditions that can be treated with DNS.

Nomenclature

Symbols

a	model constant, $a \equiv (g\beta/\sigma_u\alpha)$
A	model constant, $A \equiv (0.42^{1/2}1.5^{3/4})/(aPr^{1/2})$
B	reaction rate preexponential factor (equation 9)
c	reaction progress variable
D	molecular mass diffusivity of deficient reactant
D_t	turbulent diffusivity
D_{th}	thermal diffusivity
g	BML model constant (equation 4)
k	mean turbulent kinetic energy
K	total mean flame stretch
K_i	mean flame stretch due to flame instabilities
K_t	mean flame stretch due to turbulent eddies
K_+	mean positive flame stretch, $K_+ \equiv \int_0^\infty \kappa p(\kappa) d\kappa$
l_F	laminar flame thickness, $l_F \equiv (D_{th}/s_L)$
l_t	turbulent flow integral length scale
L_y	characteristic length scale of wrinkling (equation 4)
Le	flame Lewis number, $Le \equiv (D_{th}/D)$
$p(Q)$	probability density function of Q
Pr	Prandtl number
Re_t	turbulent Reynolds number, $Re_t \equiv (u' l_t/\nu)$
Ri	flame Richardson number, $Ri \equiv (\Gamma D_{th}/\tau s_L^3)$
s_L	laminar flame speed
t	time
t_1	transition time in the DNS between turbulent and unstable flame behavior
T	fluid temperature
T_a	activation temperature
u'	turbulent rms velocity
u_i	x_i component of the fluid velocity
V	total volume of the computational domain
x_i	cartesian coordinate component
Y_R	reactant mass fraction
Ze	reduced activation energy, $Ze \equiv \gamma(T_a/T_b)$
α	CFM model constant (equation 1)
β	CFM model constant (equation 1)
γ	modified heat release factor, $\gamma \equiv \tau/(\tau + 1)$
γ_κ	ITNFS function from Ref. [24]
Γ	amplitude of an externally imposed acceleration field
ε	mean rate of dissipation of turbulent kinetic energy
κ	local flame stretch
Λ_n	marginal wavelength of linear laminar flame stability theory from Ref. [3]
ν	kinematic viscosity
$\dot{\omega}_R$	reaction rate (mass of reactant consummed per unit time and per unit volume)
ρ	mass density
Σ	flame surface density
$\bar{\sigma}_y$	BML flamelet orientation factor (equation 4)
τ	heat release factor, $\tau \equiv (T_b - T_u)/T_u$
τ_0	initial turbulent eddy turnover time, $\tau_0 \equiv (l_t/u')(t = 0)$
Θ	reduced temperature, $\Theta \equiv (T - T_u)/(T_b - T_u)$

Subscripts

b	value in the burnt gas
u	value in the unburnt gas

Averaging symbols

$\bar{Q}$	standard ensemble-average
$\tilde{Q}$	Favre-average, $\tilde{Q} \equiv (\overline{\rho Q}/\bar{\rho})$
$\langle Q \rangle$	volume-average, $\langle Q \rangle \equiv (\int Q dV)/V$

REFERENCES

1. Clavin, P., *Prog. Energy Combust. Sci.* 11:1–59 (1985).
2. Williams, F. A., *Combustion Theory,* 2nd ed. Benjamin Cummings, Menlo Park, CA, 1985.
3. Pelcé, P. and Clavin, P., *J. Fluid Mech.* 124:219–237 (1982).
4. Matalon, M. and Matkowsky, B. J., *J. Fluid Mech.* 124:239–259 (1982).
5. Sivashinsky, G. I., *Ann. Rev. Fluid Mech.* 15:179–199 (1983).
6. Clavin, P. and Williams, F. A., *J. Fluid Mech.* 116:251–282 (1982).
7. Searby, G. and Clavin, P., *Combust. Sci. Technol.* 46:167–193 (1986).
8. Aldredge, R. C. and Williams, F. A., *J. Fluid Mech.* 228:487–511 (1991).
9. Peters, N., *J. Fluid Mech.* 242:611–629 (1992).
10. Abdel-Gayed, R. G., Bradley, D., Hamid, M. N., and Lawes, M., in *Twentieth Symposium (International) on Combustion,* The Combustion Institute, Pittsburgh, 1984, pp. 505–512.

11. Wu, M. S., Kwon, S., Driscoll, J. F., and Faeth, G. M., *Combust. Sci. Technol.* 73:327–350 (1990).
12. Ashurst, W. T., Peters, N., and Smooke, M. D., *Combust. Sci. Technol.* 53:339–375 (1987).
13. Haworth, D. C. and Poinsot, T., *J. Fluid Mech.* 244:405–436 (1992).
14. Rutland, C. J. and Trouvé, A., *Combust. Flame* 94:41–57 (1993).
15. Trouvé, A. and Poinsot, T., *J. Fluid Mech.* 278:1–31 (1994).
16. Cambray, P. and Joulin, G., *Combust. Sci. Technol.* 97:405–428 (1994).
17. Paul, R. N. and Bray, K. N. C., in *Twenty-Sixth Symposium (International) on Combustion,* The Combustion Institute, Pittsburgh, 1996, pp. 259–266.
18. Pope, S. B., *Int. J. Eng. Sci.* 26:445–469 (1988).
19. Candel, S. M. and Poinsot, T., *Combust. Sci. and Technol.* 70:1–15 (1990).
20. Marble, F. E. and Broadwell, J. E., *The Coherent Flame Model for Turbulent Chemical Reactions,* Project Squid technical report TRW-9-PU, 1977.
21. Darabiha, N., Giovangigli, V., Trouvé, A., Candel, S. M., and Esposito, E., *France-USA Joint Workshop on Turbulent Combustion,* Springer-Verlag, New York, 1987.
22. Duclos, J. M., Veynante, D., and Poinsot, T., *Combust. Flame* 95:101–117 (1993).
23. Bray, K. N. C., *Proc. R. Soc. London, Ser. A* 431:315–335 (1990).
24. Meneveau, C. and Poinsot, T., *Combust. Flame* 86:311–332 (1991).
25. Lele, S. K., *J. Comp. Phys.* 103:16–42 (1992).
26. Poinsot, T. and Lele, S. K., *J. Comp. Phys.* 101:104–129 (1992).
27. Veynante, D. and Poinsot, T., *J. Fluid Mech.* 353:83–114 (1997).
28. Poinsot, T., Candel, S., and Trouvé, A., *Prog. Energy Combust. Sci.* 21:531–576 (1996).
29. Bray, K. N. C., *Proc. R. Soc. London, Ser. A* 451:231–256 (1995).
30. Veynante, D., Trouvé, A., Bray, K. N.C., and Mantel, T., *J. Fluid Mech.* 332:263–293 (1997).
31. Libby, P. A., *Combust. Sci. Technol.* 68:15–33 (1989).
32. Yeung, P. K., Girimaji, S. S., and Pope, S. B., *Combust. Flame* 79:340–365 (1990).